Comptes Rendus
Géoscience — Sciences de la Planète
Supplementary material to the article available at:
https://doi.org/10.5802/crgeos.176

Supplementary material: Ground deformation monitoring of the eruption offshore Mayotte

Document complémentaire : Suivi des déformations liées à l'éruption au large de Mayotte

Aline Peltier [*, a, b], **Sébastien Saur** [c], **Valérie Ballu** [d], **François Beauducel** [a], **Pierre Briole** [e], **Kristel Chanard** [a], **Denis Dausse** [d], **Jean-Bernard De Chabalier** [a], **Raphael Grandin** [a], **Perrine Rouffiac** [c], **Yann-Treden Tranchant** [d], **Maxime Bès de Berc** [f], **Simon Besançon** [a], **Patrice Boissier** [a, b], **Céleste Broucke** [a, g], **Christophe Brunet** [a, b], **Kevin Canjamalé** [a, b], **Erwan Carme** [h], **Philippe Catherine** [a, b], **Alison Colombain** [i], **Wayne Crawford** [a], **Romuald Daniel** [a], **Grégoire Dectot** [h], **Nicolas Desfete** [a, b], **Cécile Doubre** [f], **Tom Dumouch** [a], **Cyprien Griot** [a, b], **Marc Grunberg** [g], **Hélène Jund** [g], **Philippe Kowalski** [a, b], **Frédéric Lauret** [a, b], **Jacques Lebreton** [a, b], **Frédérick Pesqueira** [a, b], **Frédéric Tronel** [h], **Pierre Valty** [c] and **Jérôme van der Woerd** [f]

[a] Université Paris Cité, Institut de physique du globe de Paris, CNRS, 75005 Paris, France

[b] Observatoire volcanologique du Piton de la Fournaise, Institut de Physique du Globe de Paris, 97418 La Plaine des Cafres, France

[c] Institut national de l'information géographique et forestière, Service de Géodésie et Métrologie, 94165 Saint Mandé, France

[d] LIttoral ENvironnement et Sociétés (LIENSs) UMR7266, La Rochelle Université - CNRS, La Rochelle, France

[e] UMR 8538 CNRS - École normale supérieure - PSL Research University, Laboratoire de Géologie, 24, r. Lhomond, 75231 Paris, France

[f] Institut terre et environnement de Strasbourg, Université de Strasbourg, CNRS, UMR7063 67000 Strasbourg, France

[g] EOST/UAR 830, Université de Strasbourg/CNRS, 5 rue René Descartes, 67084 Strasbourg Cedex, France

[h] Bureau de recherches géologique et minières DAT/OMR/MAY, BP363 97646 Mamoudzou cedex, Mayotte, France

[i] Bureau de recherches géologiques et minières GR/GBS, BP 36009 45060 Orléans Cedex 2, France

E-mails: peltier@ipgp.fr (A. Peltier), Sebastien.Saur@ign.fr (S. Saur), valerie.ballu@univ-lr.fr (V. Ballu), beauducel@ipgp.fr (F. Beauducel), briole@ens.fr

* Corresponding author.

(P. Briole), chanard@ipgp.fr (K. Chanard), Denis.dausse@univ-lr.fr (D. Dausse), jbdechabalier@ipgp.fr (J.-B. De Chabalier), grandin@ipgp.fr (R. Grandin), Perrine.Rouffiac@ign.fr (P. Rouffiac), yanntreden.tranchant1@univ-lr.fr (Y.-T. Tranchant), mbesdeberc@unistra.fr (M. B. de Berc), sbesancon@ipgp.fr (S. Besançon), boissier@ipgp.fr (P. Boissier), broucke@ipgp.fr (C. Broucke), brunet@ipgp.fr (C. Brunet), canjamale@ipgp.fr (K. Canjamalé), e.carme@brgm.fr (E. Carme), caterine@ipgp.fr (P. Catherine), a.colombain@brgm.fr (A. Colombain), crawford@ipgp.fr (W. Crawford), r.daniel@ipgp.fr (R. Daniel), G.Dectot@brgm.fr (G. Dectot), desfete@ipgp.fr (N. Desfete), cecile.doubre@unistra.fr (C. Doubre), dumouch@ipgp.fr (T. Dumouch), griot@ipgp.fr (C. Griot), marc.grunberg@unistra.fr (M. Grunberg), helene.jund@unistra.fr (H. Jund), kowalski@ipgp.fr (P. Kowalski), lauret@ipgp.fr (F. Lauret), lebreton@ipgp.fr (J. Lebreton), pesqueir@ipgp.fr (F. Pesqueira), F.Tronel@brgm.fr (F. Tronel), Pierre.Valty@ign.fr (P. Valty), jerome.vanderwoerd@unistra.fr (J. van der Woerd)

Supplementary Material A. List of GNSS stations used for the monitoring in Mayotte.

Station	Owner/network	Remarks	Installation date	Data license
MAYG	CNES/REGINA	Included in the RGP network	2013-11-21	ETALAB / CC-BY 3.0
BDRL	Exagone/TERIA	Included in the RGP network	2017-10-24	ETALAB / CC-BY 3.0
GAMO	Exagone/TERIA	Included in the RGP network	2017-10-24	ETALAB / CC-BY 3.0
KAWE	Précision Topo/Réseau Lél@	Included in the RGP network	2017-09-30	ETALAB / CC-BY 3.0
MTSA	Précision Topo/Réseau Lél@	-	2017-09-30	Restricted
PORO	Précision Topo/Réseau Lél@	-	2017-09-30	Restricted
GLOR	OVPF-IPGP	Installed in the frame of the REVOSIMA	2019-03-13	CC-BY 4.0
PMZI	OVPF-IPGP	Installed in the frame of the REVOSIMA	2019-03-07	CC-BY 4.0
KNKL	OVPF-IPGP	Installed in the frame of the REVOSIMA	2019-03-05	CC-BY 4.0
MTSB	OVPF-IPGP	Installed in the frame of the REVOSIMA	2019-04-08	CC-BY 4.0
DSUA	Météo France / Université de la Réunion	-	2018-05-25	open data
NOSY	Météo France / Université de la Réunion	-	2020-02-27	open data

Supplementary Material B. SBE37 and A0A RBR deployments during successive MAYOBS campaigns [Rinnert et al., 2019]. The SBE37 sensor network was later completed by an A0A pressure gauge first deployed during the October 2020–April 2021 period (A0A1) and redeployed during the April 2021–September 2021 period (A0A2).

	Retrieval cruise	Name	Lon. (°)	Lat. (°)	Depth (m)	
Feb-19 - May-19	Mayobs1	MOSE	45.190	-12.963	3520	
		MONN	45.558	-12.493	3180	
		MOSO	45.459	-13.018	2530	
		MONO	45.392	-12.651	1600	
		MONE	45.804	-12.665	3510	
		MOCE	45.634	-12.807	3200	
May-19 - Sep-19	Mayobs6	MOFA	45.567	-12.873	2702	
		MODA	45.593	-12.671	3290	
		MOSA	45.414	-12.995	2250	
		MONA	45.409	-12.596	2030	
		MOVA	45.765	-12.922	3427	
Dec-19 - May-20	Mayobs13	MODF	45.593	-12.671	3245	
		MOAF	45.820	-12.963	3511	
		MOCF	45.411	-12.784	1715	
		MOSF	45.459	-13.018	2533	
May-20 - Oct-20	Mayobs15	MOAG	45.818	-12.957	3516	
		MOBG	45.622	-12.843	3114	
		MOCG	45.411	-12.784	1721	
		MOSG	45.517	-13.025	2533	
		MODG	45.593	-12.671	3258	
Oct-20 - Jan-21	Mayobs17	MOBH	42.623	-12.842	3110	A0A1
		MOCH	45.411	-12.784	1712	
		MOSH	45.456	-13.025	2532	
		MODH	45.593	-12.671	3248	
Feb-21 - Apr-21	Mayobs18	MOAI	45.82	-12.962	3515	
		MOBI	45.617	-12.833	3115	
		MOCI	45.411	-12.784	1713	
		MOSI	45.458	-13.020	2528	
		MODI	45.592	-12.671	3247	
Apr-21 - Sep-21	Mayobs21	MOAJ	45.82	-12.962	3517	A0A2
		MOBJ	45.622	-12.842	3105	
		MOCJ	45.412	-12.784	1718	
		MOSJ	45.459	-13.021	2523	
		MODJ	45.593	-12.671	3246	

Supplementary Material C. Location of SBE37 pressure gauges records (red diamonds) during the other MAYOBS campaigns (see Supplementary Material B), used for source modeling (see Supplementary Figures H1 to H4). Black star indicates the eruption location.

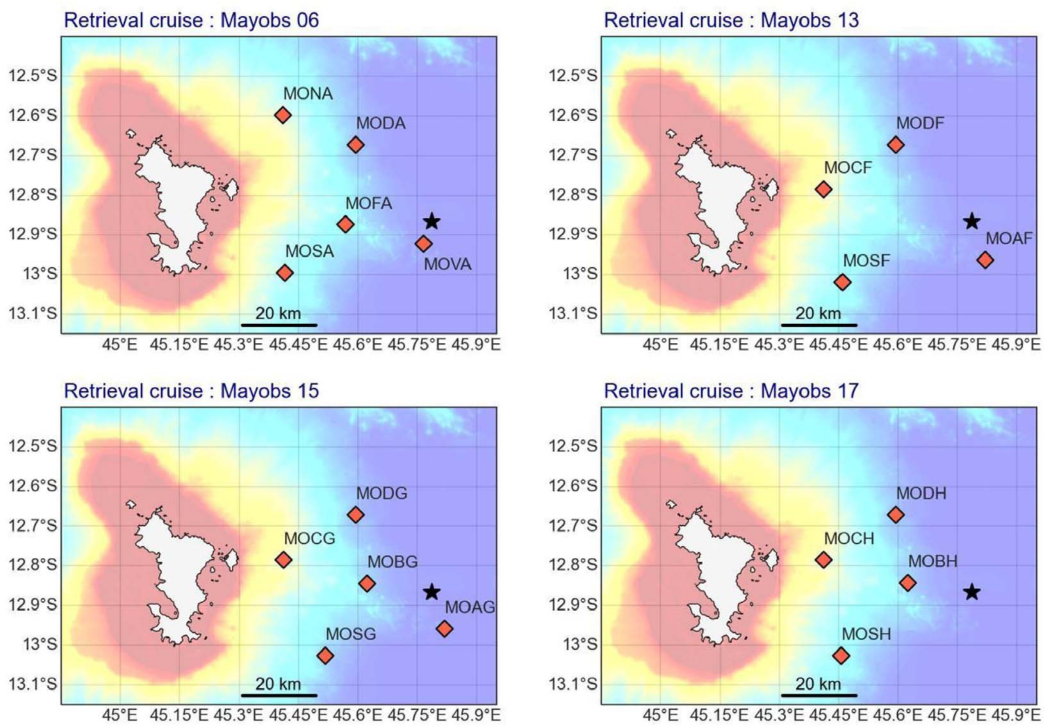

Supplementary Material D. Bottom pressure differences between collocated SBE37 sensors (MOCH and MOCI deployments) and the A0A1 drift-corrected data records during October 2020–February 2021 and February 2021–April 2021 periods.

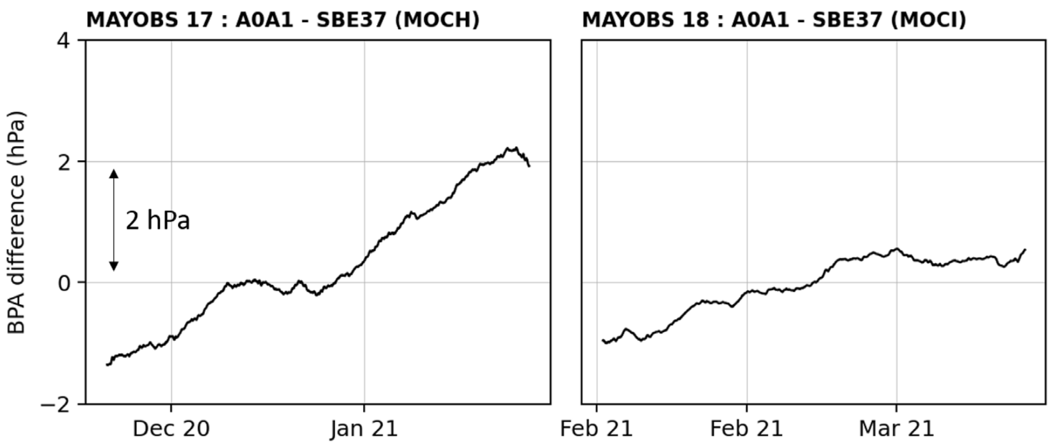

Supplementary Material E. Bottom pressure anomalies and associated trends during the other MAYOBS campaigns used for source modeling (see Supplementary Figures H1 to H4) (see Figure 3 for complete legend).

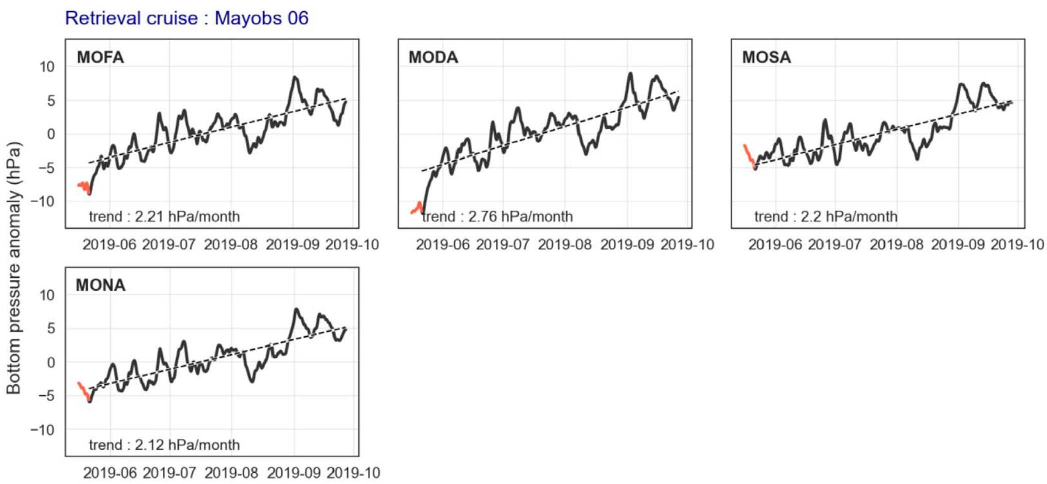

Bottom pressure anomalies from May 16, 2019 to September 26, 2019

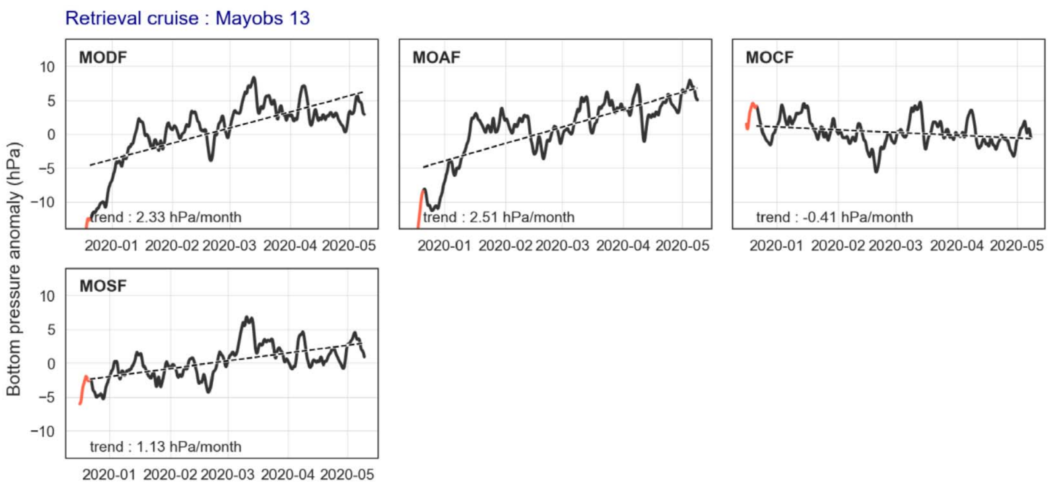

Bottom pressure anomalies from December 16, 2019 to May 8, 2020

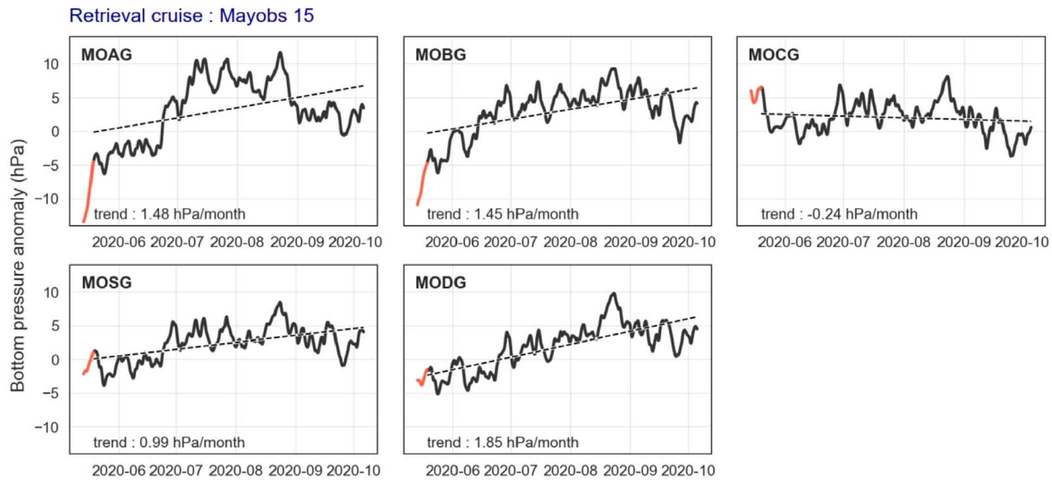

Bottom pressure anomalies from May 13, 2020 to October 5, 2020

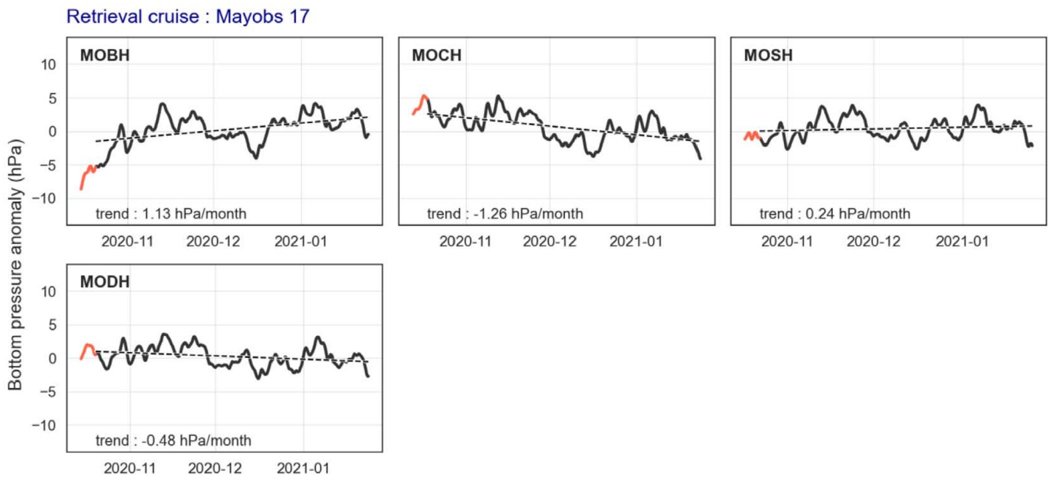

Bottom pressure anomalies from October 17, 2020 to January 23, 2021

Supplementary Material F. Time series of daily solutions of eastward (top), northward (middle), and vertical (bottom) ground displacements as recorded by GNSS stations of Mayotte, Grande Glorieuse (GLOR), and Madagascar (DSUA, NOSY), between January 1, 2017 and December, 31 2021. In blue: the raw data, in red: the data corrected from plate motion and harmonic.

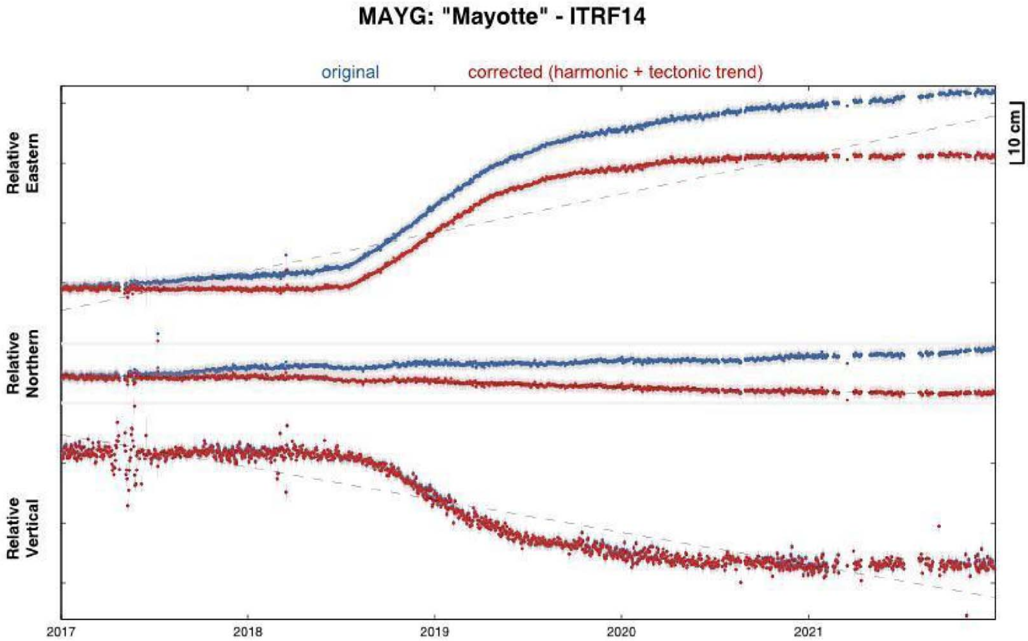

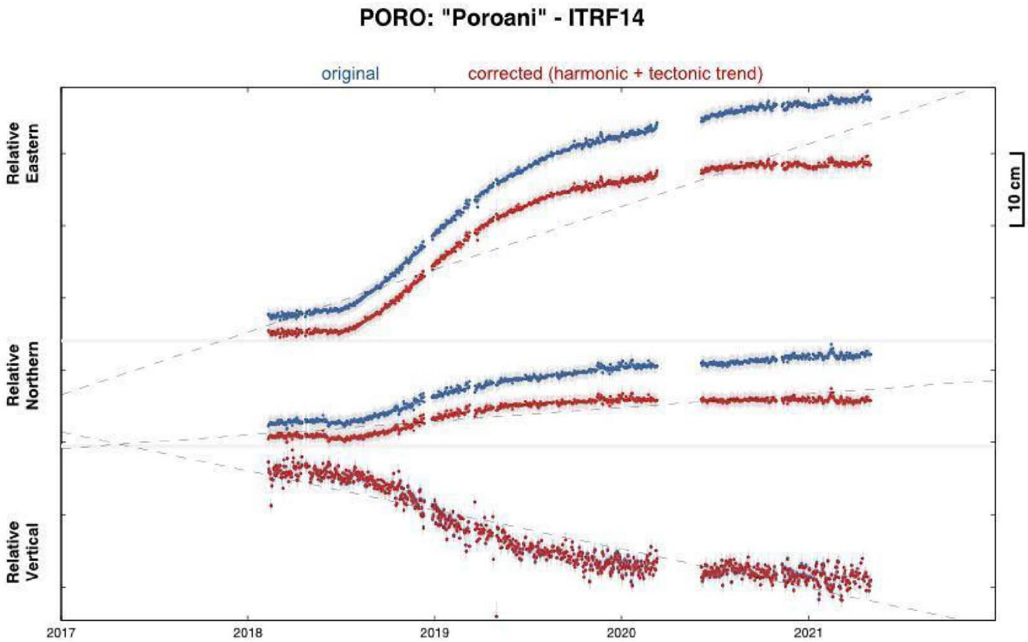

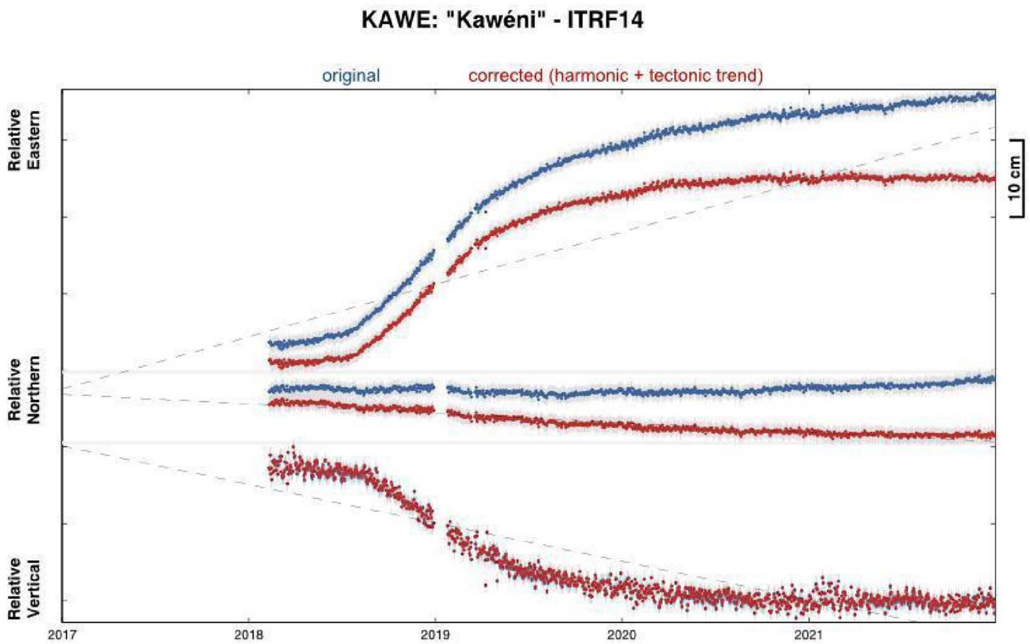
KAWE: "Kawéni" - ITRF14
original
corrected (harmonic + tectonic trend)
Relative Eastern
Relative Northern
Relative Vertical
10 cm
2017
2018
2019
2020
2021

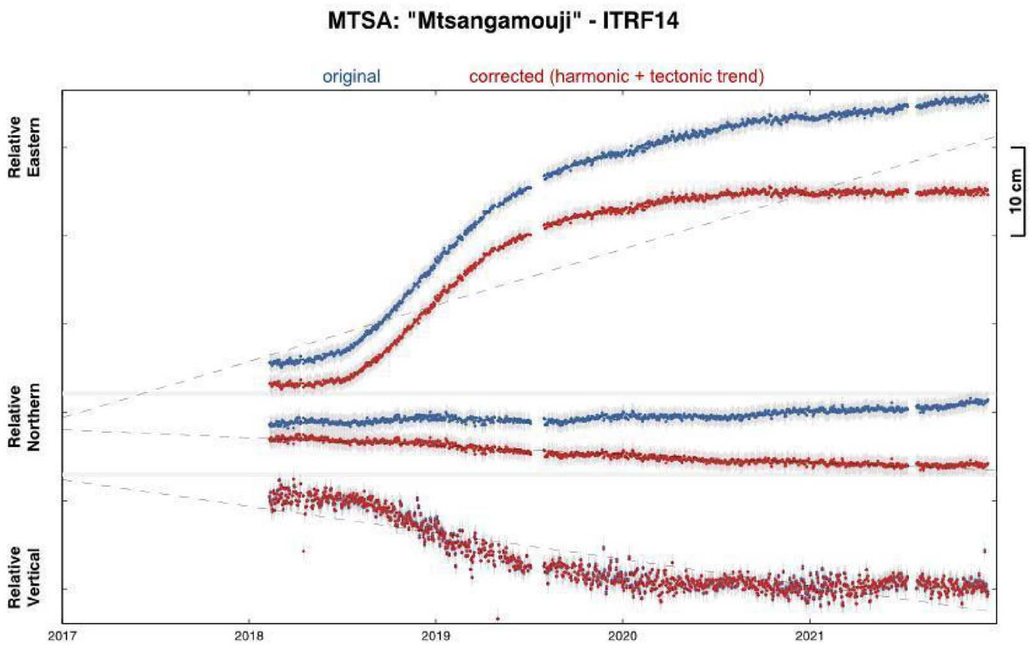
MTSA: "Mtsangamouji" - ITRF14
original
corrected (harmonic + tectonic trend)
Relative Eastern
Relative Northern
Relative Vertical
10 cm
2017
2018
2019
2020
2021

GAMO: "M''Tsangamouji" - ITRF14

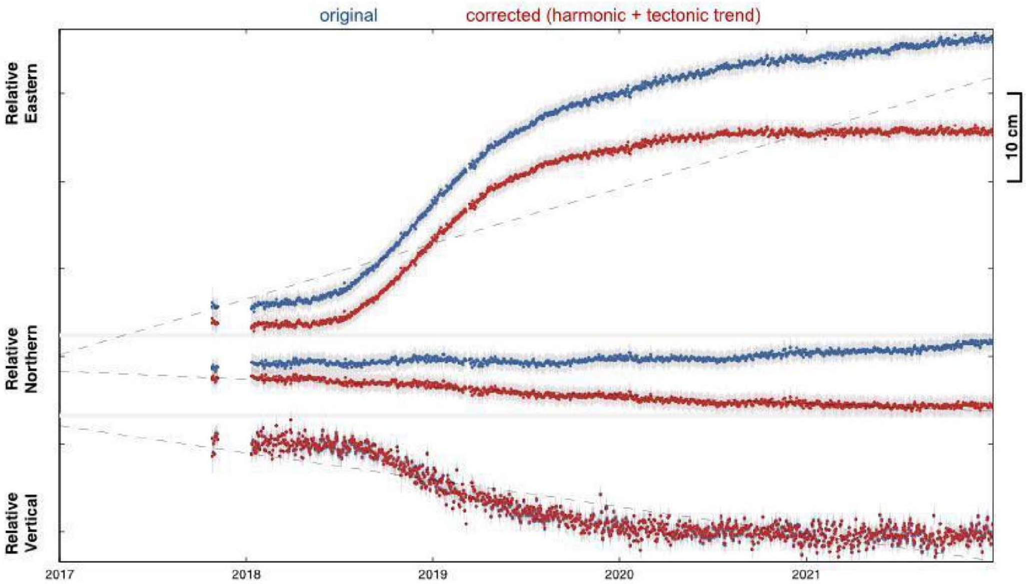

BDRL: "Bandrélé" - ITRF14

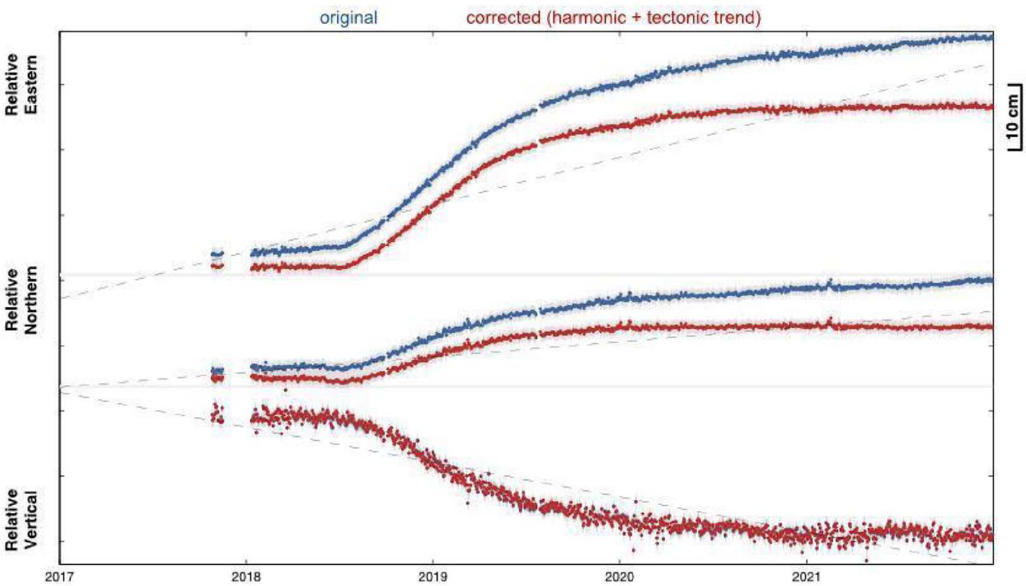

MTSB: "Mstamboro / Mtsahara" - ITRF14

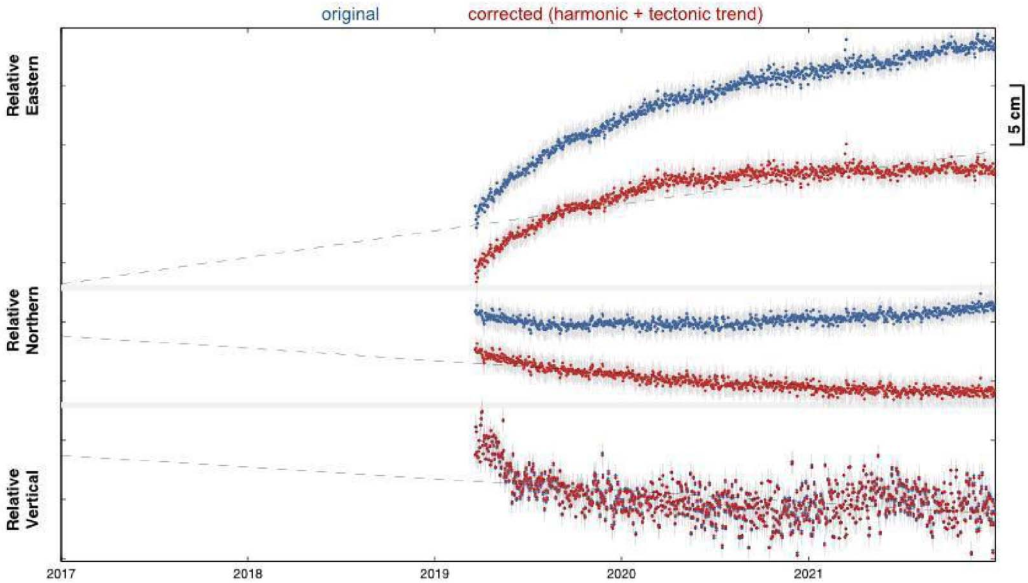

KNKL: "Kani Keli" - ITRF14

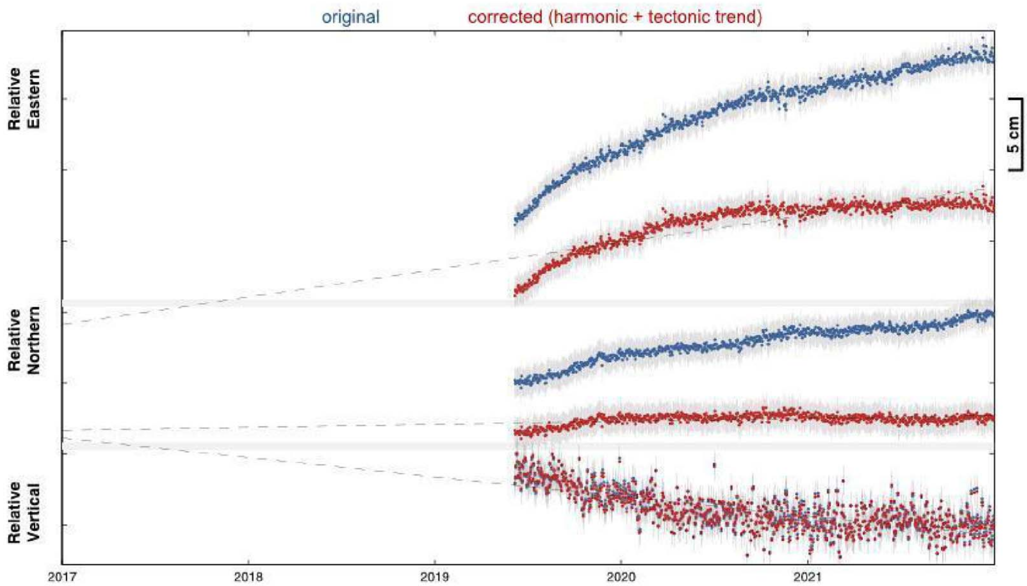

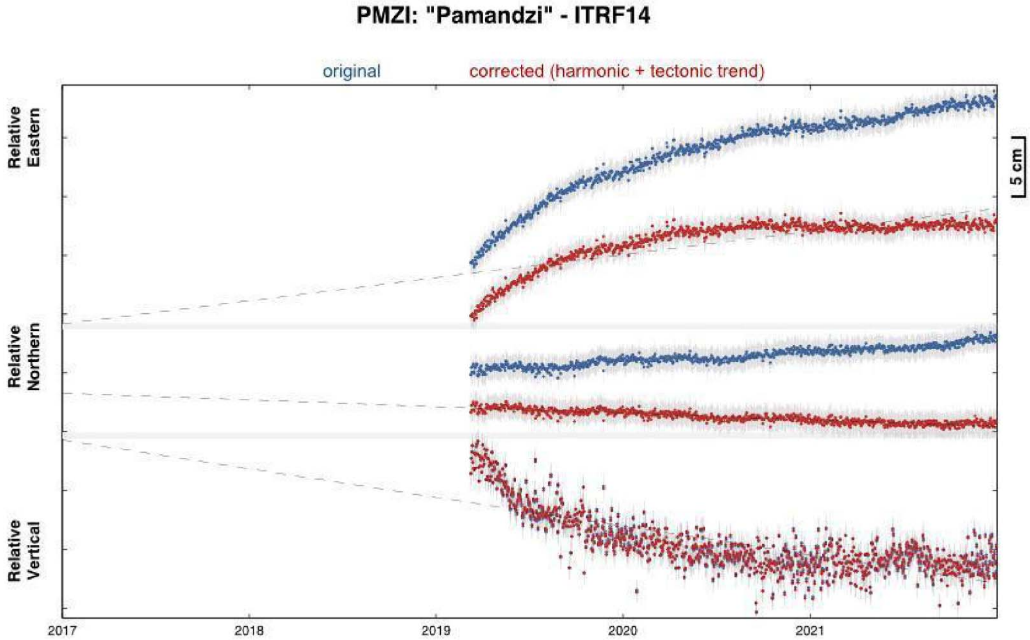
PMZI: "Pamandzi" - ITRF14
original
corrected (harmonic + tectonic trend)
Relative Eastern
Relative Northern
Relative Vertical
5 cm
2017
2018
2019
2020
2021

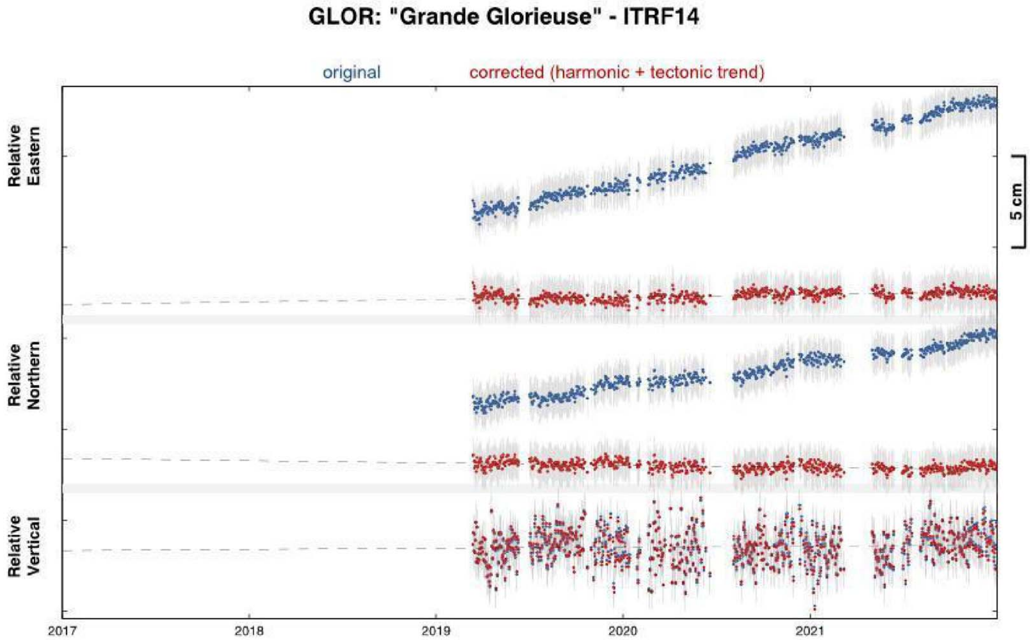
GLOR: "Grande Glorieuse" - ITRF14
original
corrected (harmonic + tectonic trend)
Relative Eastern
Relative Northern
Relative Vertical
5 cm
2017
2018
2019
2020
2021

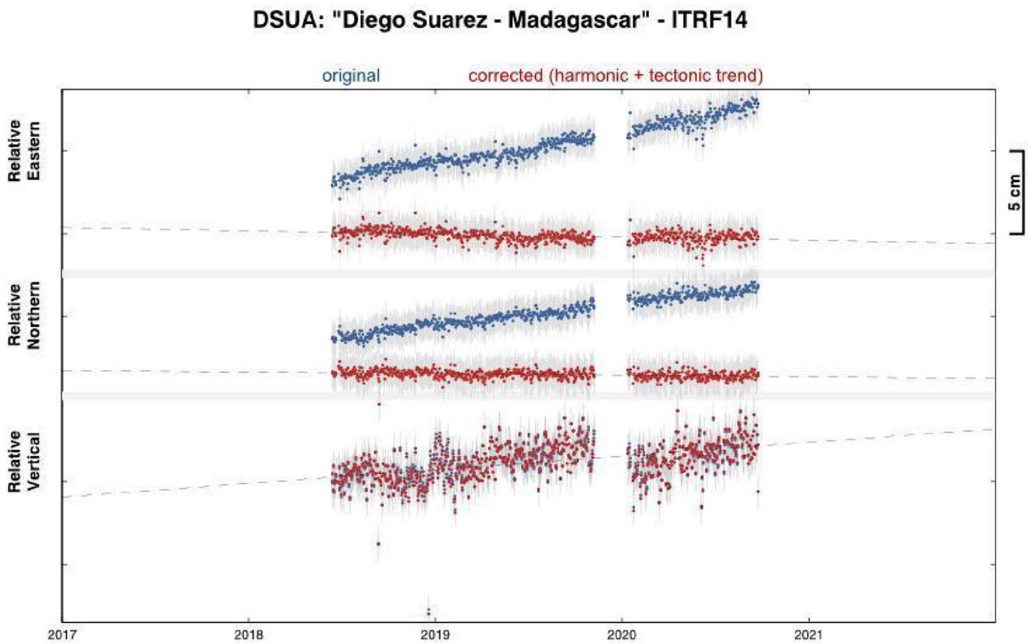
DSUA: "Diego Suarez - Madagascar" - ITRF14
original
corrected (harmonic + tectonic trend)
Relative Eastern
Relative Northern
Relative Vertical
5 cm
2017
2018
2019
2020
2021

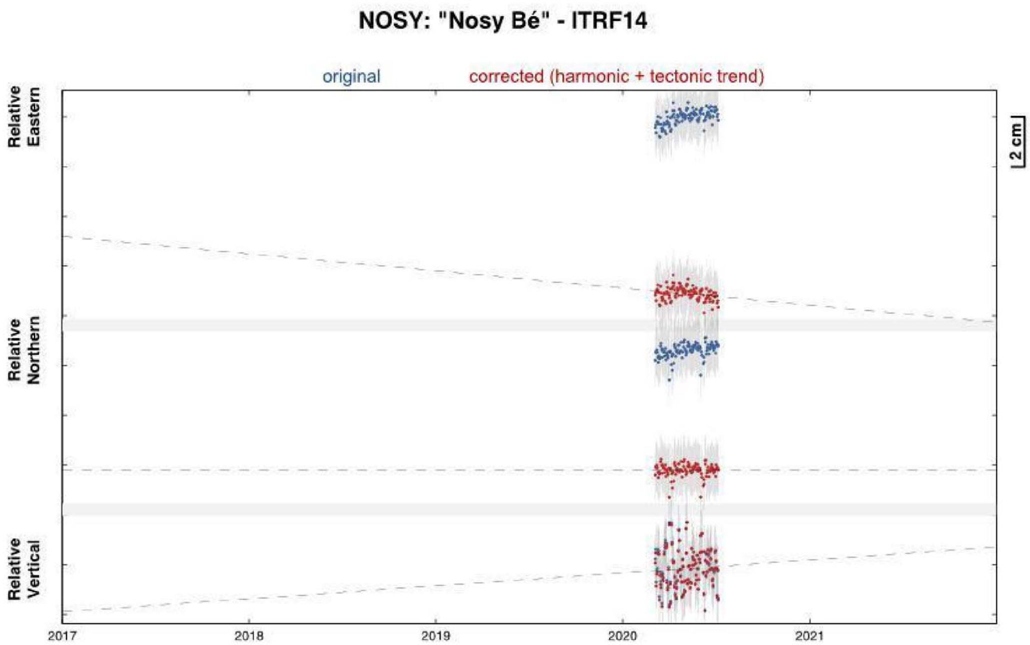
NOSY: "Nosy Bé" - ITRF14
original
corrected (harmonic + tectonic trend)
Relative Eastern
Relative Northern
Relative Vertical
2 cm
2017
2018
2019
2020
2021

Supplementary Material G

Velocities observed and calculated for the best models at each station: East, North, and Up component for GNSS and OBP Up component. Dark gray cell background stands for a residual greater than 2 sigmas of data uncertainty, light gray for residual greater than 1 sigma but less than 2 sigmas.

Supplementary Table G1. GNSS velocity components observed and calculated for each 1-year period of observation (from January 1st to December 31), as used in Figure 8

station		2018		2019		2020		2021	
		obs (mm/yr)	calc	obs (mm/yr)	calc	obs (mm/yr)	calc	obs (mm/yr)	calc
BDRL	E	87.6 ± 5	100.1	117.5 ± 5	98.3	25.3 ± 5	21.6	5.2 ± 5	3.8
	N	28.8 ± 5	17.5	39.7 ± 5	15.1	2.3 ± 5	-0.4	-1.5 ± 5	-1.5
	U	-65.2 ± 10	-65.3	-84.4 ± 10	-73.8	-20.2 ± 10	-20.3	-0.8 ± 10	-1.5
DSUA	E	-0.3 ± 5	-4.0	-3.9 ± 5	-3.7	0.4 ± 5	-0.7		
	N	0.4 ± 5	-0.6	0.6 ± 5	-0.6	-0.5 ± 5	-0.1		
	U	-10.5 ± 12	-0.4	18.5 ± 10	-0.4	26.9 ± 10	-0.1		
GAMO	E	94.1 ± 5	82.4	99.7 ± 5	80.7	17.9 ± 5	16.7	2.1 ± 5	2.2
	N	-8.8 ± 5	-7.1	-13.0 ± 5	-9.9	-6.5 ± 5	-5.1	-1.5 ± 5	-1.3
	U	-40.4 ± 10	-44.9	-49.7 ± 10	-49.9	-5.7 ± 10	-12.4	1.8 ± 10	-0.7
GLOR	E			-4.1 ± 5	-8.9	4.2 ± 5	-1.6	1.0 ± 5	-0.2
	N			0.1 ± 5	-7.2	-1.0 ± 5	-1.3	0.8 ± 5	-0.2
	U			4.6 ± 10	-2.1	2.6 ± 10	-0.4	10.1 ± 10	-0.0
KAWE	E	111.4 ± 5	109.1	99.8 ± 5	104.3	18.8 ± 5	20.2	0.2 ± 5	2.9
	N	-14.1 ± 5	-10.8	-16.3 ± 5	-15.4	-7.7 ± 5	-8.1	-2.3 ± 5	-2.2
	U	-76.7 ± 10	-75.7	-76.3 ± 10	-83.7	-18.9 ± 10	-20.5	-6.4 ± 10	-1.2
KNKL	E			64.8 ± 5	81.3	20.4 ± 5	18.7	4.0 ± 5	3.2
	N			21.6 ± 5	17.1	2.9 ± 5	1.4	-0.6 ± 5	-0.8
	U			-38.4 ± 10	-52.0	-14.5 ± 10	-14.5	-2.3 ± 10	-1.1
MAYG	E	88.6 ± 5	117.1	101.2 ± 5	111.2	18.5 ± 5	21.2	2.6 ± 5	3.2
	N	-8.2 ± 5	-8.6	-8.7 ± 5	-13.7	-7.1 ± 5	-8.4	-2.5 ± 5	-2.5
	U	-65.7 ± 10	-86.7	-85.7 ± 10	-95.8	-17.4 ± 10	-23.5	0.7 ± 10	-1.5
MTSA	E	105.3 ± 5	81.4	99.6 ± 5	79.8	19.3 ± 5	16.5	2.4 ± 5	2.2
	N	-6.5 ± 5	-7.0	-12.8 ± 5	-9.7	-7.4 ± 5	-5.0	-2.7 ± 5	-1.2
	U	-42.8 ± 10	-44.1	-47.4 ± 10	-49.0	-7.8 ± 10	-12.2	2.0 ± 10	-0.7
MTSB	E			73.9 ± 5	76.6	15.3 ± 5	15.0	2.4 ± 5	1.8
	N			-24.1 ± 5	-19.6	-9.0 ± 5	-6.9	-2.2 ± 5	-1.3
	U			-63.3 ± 10	-47.4	-10.6 ± 10	-11.2	-2.9 ± 10	-0.6
PMZI	E			71.5 ± 5	114.8	16.0 ± 5	21.9	3.5 ± 5	3.4
	N			-5.2 ± 5	-9.9	-5.9 ± 5	-7.9	-2.6 ± 5	-2.6
	U			-87.0 ± 10	-102.7	-25.8 ± 10	-25.5	-2.0 ± 10	-1.7
PORO	E	94.8 ± 5	91.7	110.8 ± 5	90.6	24.7 ± 5	20.1		
	N	22.8 ± 5	12.8	23.9 ± 5	10.6	-0.6 ± 5	-0.9		
	U	-56.1 ± 10	-55.0	-68.1 ± 10	-62.0	-13.1 ± 10	-16.9		

Supplementary Table G2. GNSS and OBP velocity components observed and calculated for each period of OBP campaigns (the name of the campaign refers to the retrieval cruise), as used in Figures 10, 11 and Supplementary Material H

station		Mayobs1		Mayobs6		Mayobs13		Mayobs15		Mayobs17	
		obs (mm/yr)	calc	obs (mm/yr)	calc	obs (mm/yr)	calc	obs (mm/yr)	calc	obs (mm/yr)	calc
	E	35.0 ± 5	30.5	38.5 ± 5	35.8	21.0 ± 5	18.8	11.8 ± 5	10.7	-2.0 ± 5	-1.5
BDRL	N	9.8 ± 5	3.1	7.9 ± 5	0.9	0.6 ± 5	-1.2	0.5 ± 5	-0.0	1.7 ± 5	-1.0
	U	-12.2 ± 10	-16.2	-23.3 ± 10	-23.0	-13.3 ± 10	-12.5	-6.7 ± 10	-6.5	-2.8 ± 10	0.2
	E	-1.4 ± 5	-3.2	4.2 ± 5	-1.9	2.2 ± 5	-1.0	5.6 ± 5	-0.3		
DSUA	N	0.6 ± 5	-0.5	-2.8 ± 5	-0.3	-0.9 ± 5	-0.2	-0.6 ± 5	-0.1		
	U	13.9 ± 10	-0.5	6.7 ± 10	-0.2	12.0 ± 10	-0.1	9.7 ± 10	-0.0		
	E	31.4 ± 5	26.1	32.8 ± 5	28.4	15.9 ± 5	14.6	8.8 ± 5	7.7	-1.9 ± 5	-1.5
GAMO	N	-1.7 ± 5	-1.7	-7.4 ± 5	-5.3	-6.7 ± 5	-3.8	-2.0 ± 5	-1.9	-0.9 ± 5	-0.4
	U	-7.4 ± 10	-12.4	-14.2 ± 10	-15.6	-9.3 ± 10	-8.3	-0.8 ± 10	-3.9	-10.9 ± 10	0.1
	E	1.1 ± 5	-7.2	2.9 ± 5	-4.3	1.1 ± 5	-2.2	6.4 ± 5	-0.7	-0.6 ± 5	0.1
GLOR	N	-1.3 ± 5	-7.6	-4.5 ± 5	-3.9	-4.9 ± 5	-2.1	-2.5 ± 5	-0.6	1.6 ± 5	0.1
	U	-7.4 ± 10	-2.8	6.3 ± 10	-1.2	-6.9 ± 10	-0.6	-1.7 ± 10	-0.1	-5.2 ± 10	0.0
	E	31.3 ± 5	32.2	34.1 ± 5	36.1	18.3 ± 5	18.2	10.1 ± 5	10.4	-3.0 ± 5	-2.4
KAWE	N	-2.2 ± 5	-2.2	-10.9 ± 5	-7.9	-6.4 ± 5	-5.6	-5.5 ± 5	-3.2	-0.9 ± 5	-0.8
	U	-19.5 ± 10	-17.8	-20.2 ± 10	-24.5	-15.9 ± 10	-12.8	-9.6 ± 10	-6.8	0.7 ± 10	0.3
	E			34.1 ± 5	30.3	17.0 ± 5	16.2	10.9 ± 5	8.6	-0.8 ± 5	-1.1
KNKL	N			5.8 ± 5	2.6	0.6 ± 5	0.2	0.6 ± 5	0.7	-0.7 ± 5	-0.7
	U			-9.2 ± 10	-17.2	-20.7 ± 10	-9.5	-5.3 ± 10	-4.5	-3.5 ± 10	0.1
	E	33.0 ± 5	33.9	32.3 ± 5	38.5	16.9 ± 5	19.4	9.8 ± 5	11.4	-0.9 ± 5	-2.6
MAYG	N	-2.3 ± 5	-1.7	-6.2 ± 5	-7.9	-5.5 ± 5	-5.8	-3.8 ± 5	-3.4	0.0 ± 5	-1.1
	U	-15.8 ± 10	-19.5	-20.9 ± 10	-27.6	-14.5 ± 10	-14.4	0.6 ± 10	-8.0	-5.5 ± 10	0.4
	E	30.5 ± 5	25.9	33.4 ± 5	28.1	16.6 ± 5	14.4	10.8 ± 5	7.6	-3.1 ± 5	-1.5
MTSA	N	-4.3 ± 5	-1.6	-7.7 ± 5	-5.2	-6.8 ± 5	-3.7	-2.7 ± 5	-1.9	-0.8 ± 5	-0.4
	U	-9.6 ± 13	-12.2	-10.7 ± 10	-15.4	-8.3 ± 10	-8.2	1.2 ± 10	-3.8	-1.6 ± 10	0.1
	E	29.2 ± 5	25.6	31.9 ± 5	26.8	15.5 ± 5	13.6	9.4 ± 5	7.0	-1.4 ± 5	-1.6
MTSB	N	-10.8 ± 5	-3.7	-11.5 ± 5	-7.9	-6.7 ± 5	-5.0	-3.6 ± 5	-2.7	-2.3 ± 5	-0.2
	U	-12.0 ± 16	-12.2	-14.7 ± 10	-14.8	0.3 ± 10	-7.7	-4.2 ± 10	-3.5	7.5 ± 10	0.2
	E	25.9 ± 5	34.8	30.4 ± 5	40.0	16.1 ± 5	20.1	10.3 ± 5	12.0	-2.6 ± 5	-2.6
PMZI	N	0.4 ± 5	-1.1	-6.7 ± 5	-7.2	-3.8 ± 5	-5.6	-1.7 ± 5	-3.2	-1.7 ± 5	-1.3
	U	-20.4 ± 10	-20.4	-25.1 ± 10	-29.6	-13.8 ± 10	-15.4	-12.7 ± 10	-8.7	1.9 ± 10	0.4
	E	31.7 ± 5	28.4	37.3 ± 5	32.8	17.0 ± 5	17.3	12.4 ± 5	9.5	-2.6 ± 5	-1.4
PORO	N	2.2 ± 5	2.3	4.2 ± 5	0.1	-2.9 ± 5	-1.3	0.9 ± 5	-0.2	1.5 ± 5	-0.8
	U	-8.3 ± 18	-14.3	-16.5 ± 10	-19.6	-6.6 ± 13	-10.7	1.1 ± 10	-5.3	-4.6 ± 10	0.1
MOCE	U	-75.7 ± 26	-62.2								
MONE	U	-64.6 ± 34	-95.2								
MONN	U	-32.4 ± 32	-34.9								
MONO	U	-52.0 ± 32	-26.6								
MOSE	U	-101.4 ± 28	-102.9								
MOSO	U	-42.4 ± 27	-31.7								
MODA	U			-108.0 ± 20	-72.7						
MOFA	U			-88.9 ± 19	-92.7						
MONA	U			-92.9 ± 17	-34.5						
MOSA	U			-102.3 ± 18	-49.1						
MOAF	U					-90.0 ± 19	-86.2				
MOCF	U					23.9 ± 17	-24.1				
MODF	U					-77.0 ± 20	-33.1				
MOSF	U					-44.9 ± 18	-31.9				
MOAG	U							-47.0 ± 35	-43.3		
MOBG	U							-46.1 ± 22	-46.2		
MOCG	U							15.5 ± 20	-16.1		
MODG	U							-84.4 ± 20	-21.2		
MOSG	U							-38.7 ± 18	-27.3		
MOBH	U									-24.3 ± 20	1.1
MOCH	U									40.7 ± 19	0.8
MODH	U									21.4 ± 16	20.1
MOSH	U									-2.9 ± 18	0.2

Supplementary Material H

Equivalent of Figures 10 and 11 in the main text for other OBP campaigns from 2019 to 2021. *(top)* Comparison of source modeling location as probability density levels using only GNSS data (blue contours) and using both GNSS and OBP data (red contours). *(bottom)* Best source modeling radial profiles from joint inversion of GNSS and OBP data. See Figures 10 and 11 for full legend, and Table G2 for velocity values.

As shown in Figure 9, the deployment of OBP was carried out after the occurrence of the maximum deformation, when the source flow rate already started to decrease. All the following campaigns of OBP recovery/deployment correspond to periods with lower and lower flux values. Given the large errors in the observations and especially for pressure data, this leads to increasingly large uncertainties in the calculated model. It should also be noted that the durations between each campaign are relatively short so the signal-to-noise ratio of the data does not allow for optimal source modeling, at least not with the same performance as for the one-year period.

Supplementary Figure H1 (May 16, 2019 to September 26, 2019) shows very similar sources and suggests OBP data do not modify the GNSS-only modeling result. This might be due to the OBP network configuration, as the 4 OBP are all located westward of the volcano.

Supplementary Figure H2 (December 16, 2019 to May 8, 2020) has a better network configuration and indicates that OBP data tends to pull the source upwards, with a shallower solution and larger horizontal *a posteriori* uncertainties.

Supplementary Figure H3 (May 13, 2020 to October 5, 2020) also suggests that OBP stations pull the source upwards, in addition to "maintain" the source's horizontal location in the vicinity of the volcano.

Supplementary Figure H4 (October 17, 2020 to January 23, 2021) shows results that should be interpreted with caution, as the signal-to-noise ratio is very low for both GNSS and OBP data. As a result, the Bayesian inversion clearly indicates that there is no single source able to report observations. In particular, solutions exist to the west of Mayotte for both data inversions (GNSS with or without OBP). The joint inversion (GNSS+OBP) still shows a cloud of solutions at shallow depths in the volcano area, but this is probably related to the position of the stations.

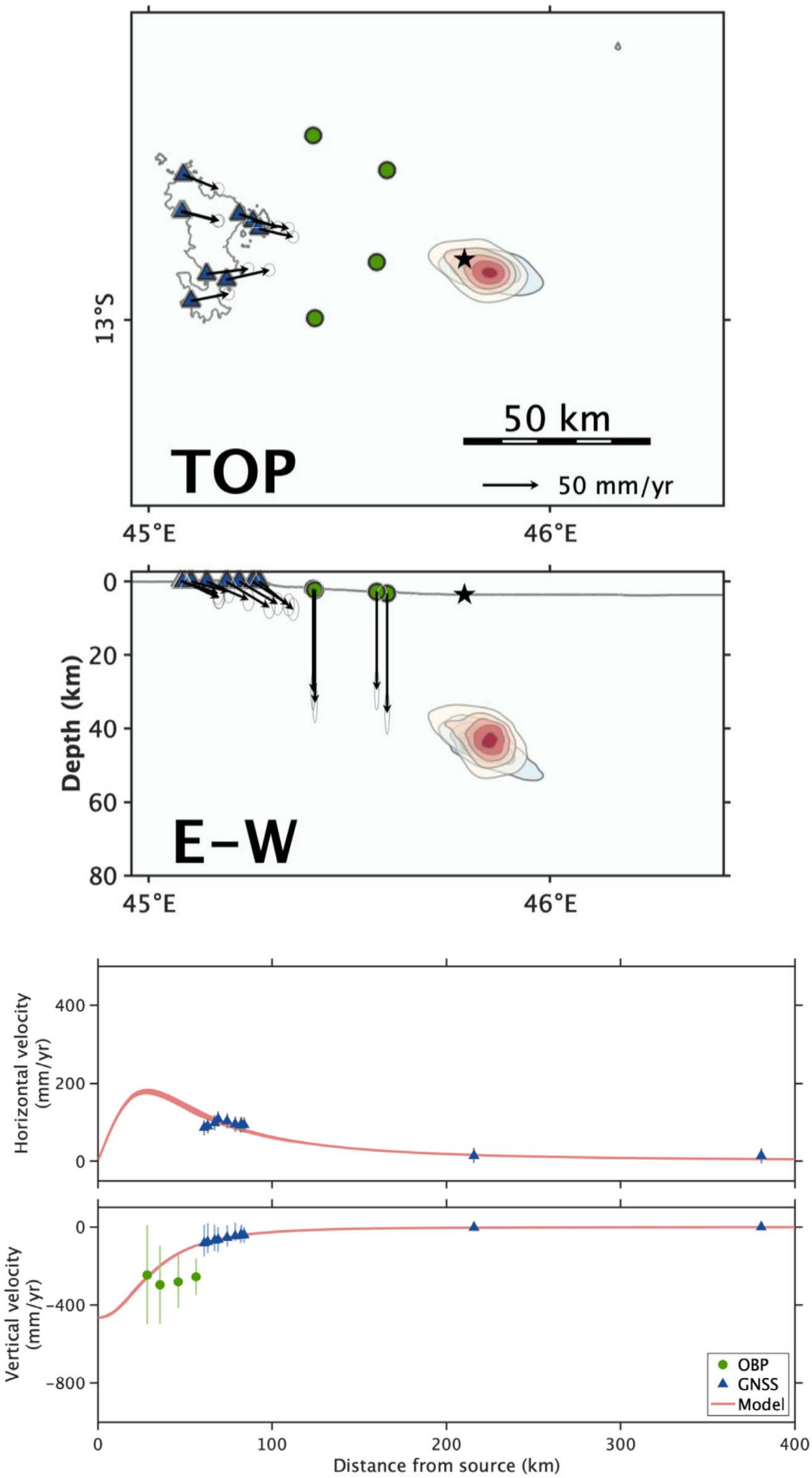

Supplementary Figure H1. GNSS/OBP data and models between May 16, 2019 and September 26, 2019.

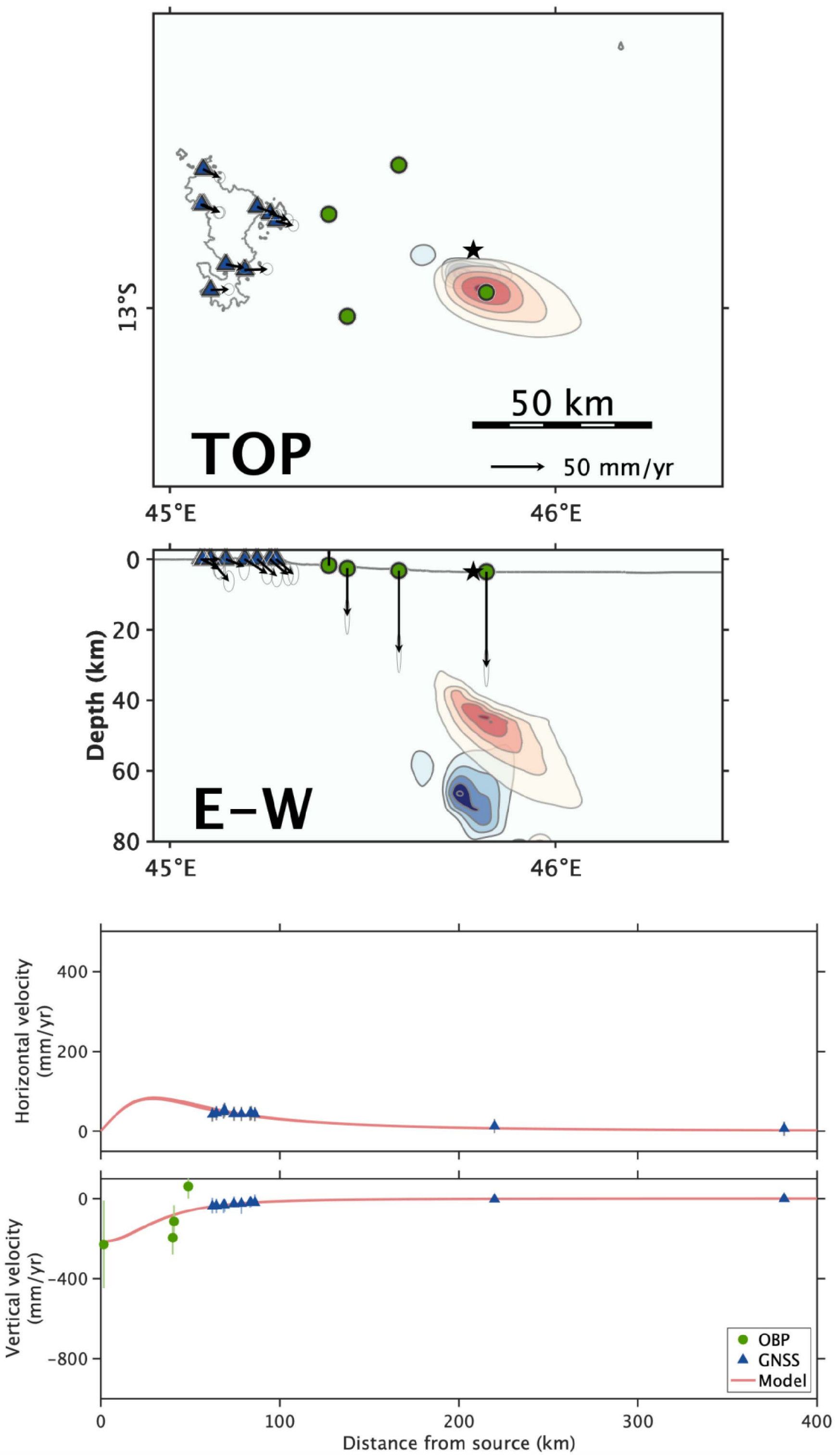

Supplementary Figure H2. GNSS/OBP data and models between December 16, 2019 and May 8, 2020.

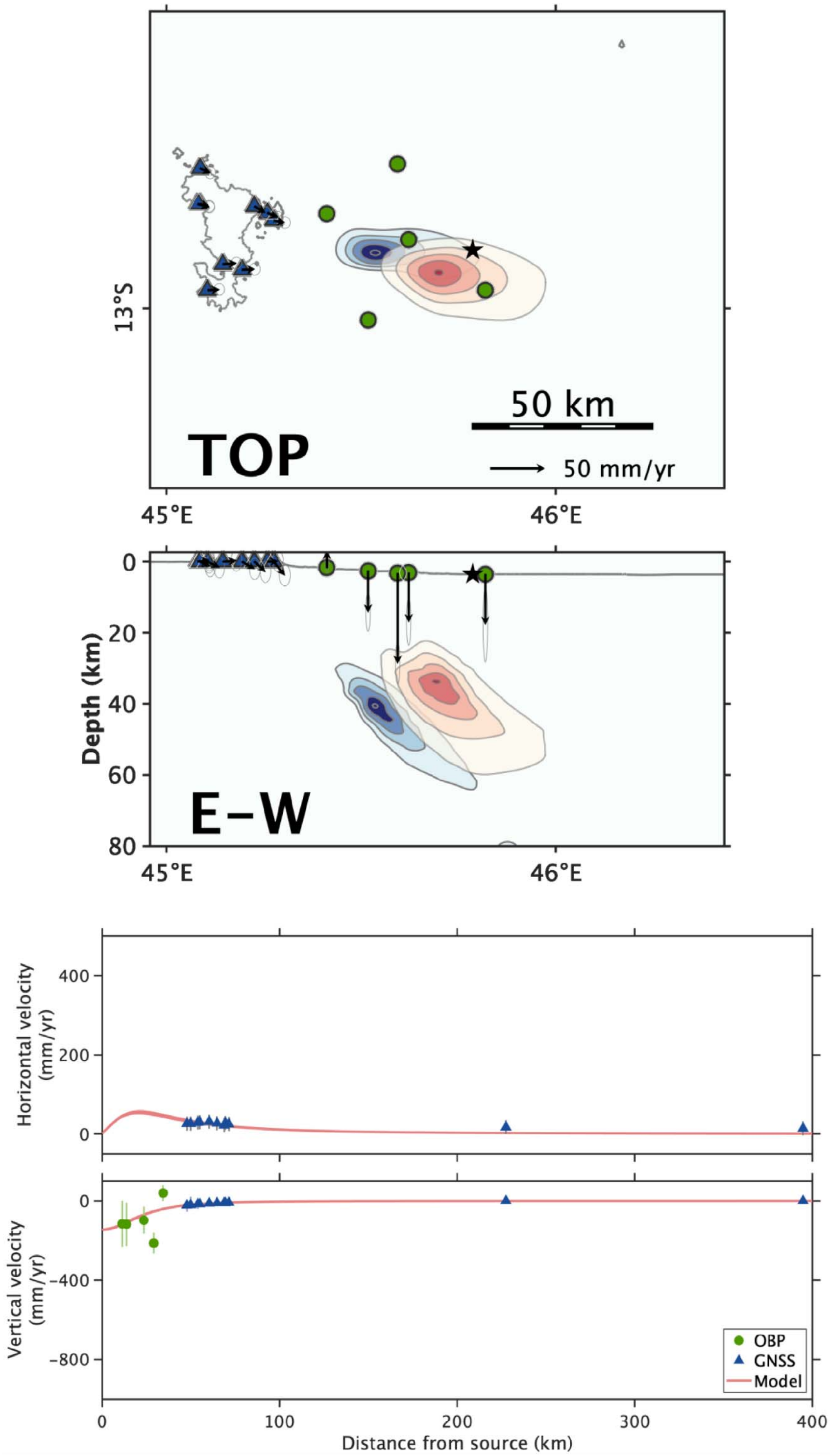

Supplementary Figure H3. GNSS/OBP data and models between May 13, 2020 and October 5, 2020.

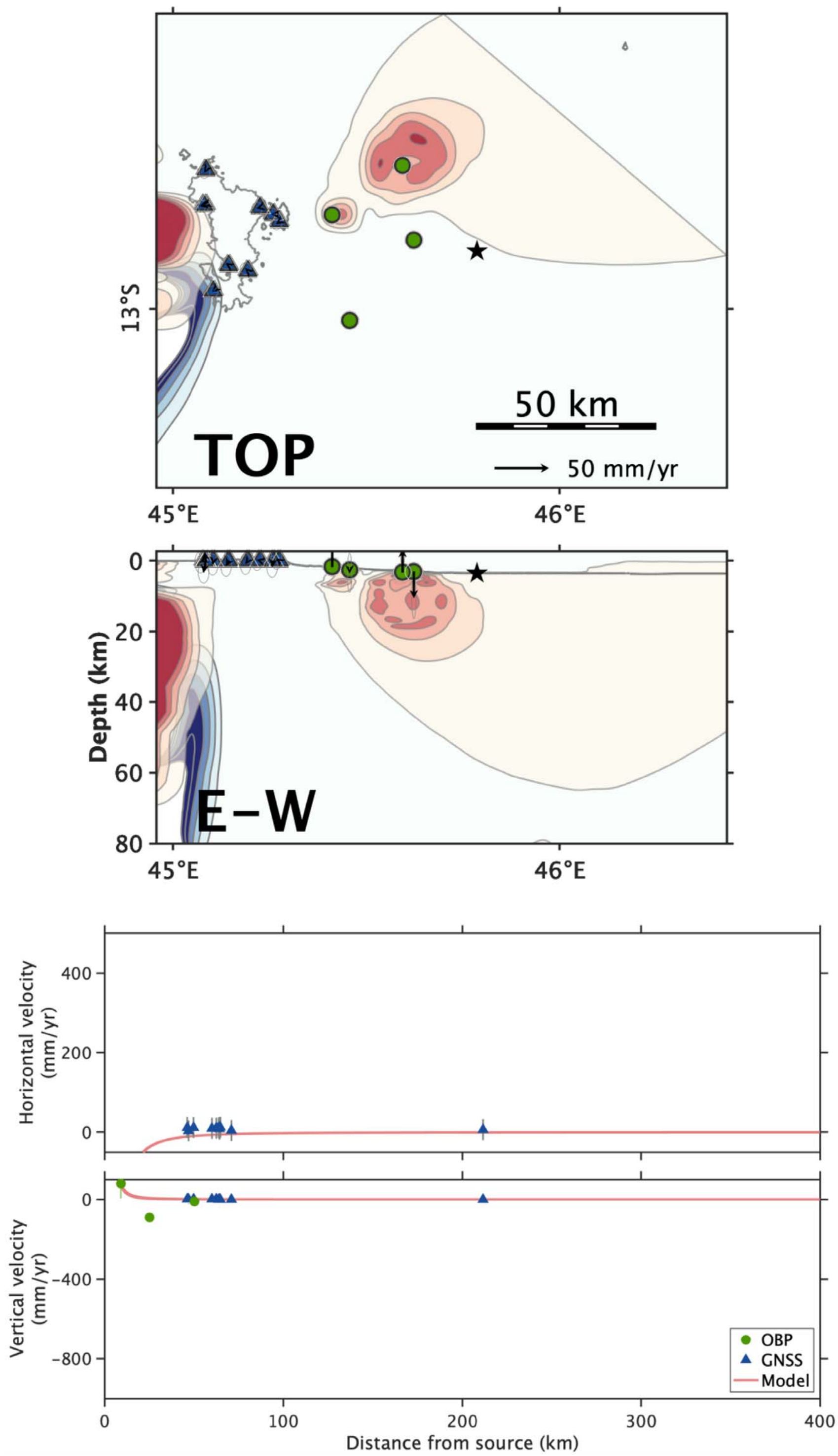

Supplementary Figure H4. GNSS/OBP data and models between October 17, 2020 and January 23, 2021.

Supplementary Material I. Source location estimated from GNSS for years 2018 to 2021 (see Figure 7 for complete legend), using a tectonic trend correction of +21.20 mm/yr east and +12.5 mm/yr north that minimizes the northern residual for year 2021.